JMEPEG (2007) 16:672–679
DOI: 10.1007/s11665-007-9098-z

1059-9495/$19.00

Modeling Microstructural Evolution During Dynamic Recrystallization of Alloy D9 Using Artificial Neural Network

Sumantra Mandal, P.V. Sivaprasad, and R.K. Dube

(Submitted July 4, 2006; in revised form November 23, 2006)

An artificial neural network (ANN) model was developed to predict the microstructural evolution of a 15Cr-15Ni-2.2Mo-Ti modified austenitic stainless steel (Alloy D9) during dynamic recrystallization (DRX). The input parameters were strain, strain rate, and temperature whereas microstructural features namely, %DRX and average grain size were the output parameters. The ANN was trained with the database obtained from various industrial scale metal-forming operations like forge hammer, hydraulic press, and rolling carried out in the temperature range 1173-1473 K to various strain levels. The performance of the model was evaluated using a wide variety of statistical indices and the predictability of the model was found to be good. The combined influence of temperature and strain on microstructural features has been simulated employing the developed model. The results were found to be consistent with the relevant fundamental metallurgical phenomena.

Keywords artificial neural network, austenitic stainless steel, dynamic recrystallization, grain size, microstructural evolution

1. Introduction

Dynamic recrystallization (DRX) takes place most readily in low to medium stacking-fault energy materials in which (because of slow climb and cross slip) dynamic recovery is sluggish, so that the driving force for recrystallization is maintained. The DRX process mainly influences the microstructure and mechanical properties and thus the formability of the materials (Ref 1). DRX consists of, besides other elementary mechanisms, grain boundary migration, and the evolution of sub-boundaries to high angle boundaries. Depending on which of these two processes is prevalent, either grain coarsening or grain refinement occurs (Ref 2).

In our recent study, it has been shown that Alloy D9 undergoes DRX during hot working (Ref 3). Alloy D9 is a 15Cr-15Ni-2.2Mo-0.3Ti modified austenitic stainless steel, which has been selected as a candidate material for in-core applications as fuel cladding tube and hexagonal subassembly wrapper for Indian fast breeder reactors. This material has to be processed through various hot forming techniques like rolling, forging, and extrusion before it is fabricated into final components. During this processing, material undergoes shape change as well as change in microstructure that depends on the process history. In order to ensure the mechanical properties demanded from the rolled and forged product, a homogeneous and completely recrystallized structure must be achieved. Therefore, to control the microstructure in the end product, it is required to quantitatively predict the effect of processing parameters on microstructural evolution during these industrial scale metal-forming processes.

In order to make an accurate computation of the microstructure during thermo-mechanical processing, many researchers have developed several models. Sellars employed an empirical formula to study recrystallization behavior by power-law functions of the process parameters, including strain, strain rate, and deformation temperature (Ref 4). Ashby applied internal state variables to describe microstructural evolution (Ref 5). Kim and Dunne proposed a phenomenological constitutive equation considering the change of grain size (Ref 6). However, it has been observed that microstructural evolution during hot working of Alloy D9 has fuzzy characteristics (Ref 3). Therefore, it is too difficult to use a single mathematical model to represent microstructural evolution during thermo-mechanical processing of Alloy D9. Artificial neural network (ANN), in this respect, provides an efficient alternative. Artificial neural network provides a parameterized, non-linear mapping between inputs and outputs. It has the inherent capability to deal with fuzzy information, whose functional relations are not clear. Therefore, in the present study, an ANN model has been developed to predict the microstructural evolution of Alloy D9 during hot forming.

Sumantra Mandal and **P.V. Sivaprasad,** Materials Technology Division, Indira Gandhi Centre for Atomic Research, Kalpakkam, TN 603102, India; and **R.K. Dube,** Department of Materials and Metallurgical Engineering, IIT Kanpur, Kanpur, UP 208016, India. Contact e-mail: prasad@igcar.gov.in.

2. Materials and Experimental

2.1 Materials

The Alloy D9 used in this present investigation was supplied by M/s. MIDHANI, Hyderabad, India, in mill

Table 1 Chemical composition (in wt.%) of 15Cr-15Ni-2.2Mo-Ti modified austenitic stainless steel (alloy D9)

C	Mn	Si	S	P	Cr	Ni	Mo	Ti	B	Co	N
0.052	1.509	0.505	0.002	0.011	15.051	15.068	2.248	0.31	0.001	0.01	0.006

annealed condition as 30 mm diameter rods. Chemical composition of the alloy is given in Table 1. The cast ingots were hot forged and hot rolled to 30 mm diameter rounds. Cold swaging operation was performed in order to reduce the diameter of the rod to 20 mm. The cold swaged rod was then annealed in a vacuum furnace at 1323 K for 1 h in order to eliminate the work hardening effect of cold working operations as well as to get complete recrystallized structure. From this solution annealed rod, 30 mm height and 20 mm diameter compression specimens for forging operation were machined. For rolling, 24 mm thick rectangular plates were machined from the initial 30 mm hot rolled and hot forged rounds.

2.2 Thermo-Mechanical Processing

Hammer forging operations were carried out with a 250-kg pneumatic hammer in a single blow in the temperature range 1223-1423 K in steps of 50 K. Temperature during the operation was monitored based on the data obtained from cooling curve, which has been established for the present study. The mean strain rate of the forge hammer is 100 s^{-1}, which has been measured by high-speed photography. True strains of 0.1, 0.2, 0.3, 0.4, and 0.5 were imparted at each temperature in order to study the effect of strain. The specified amount of strain in each sample was achieved in a single step. As soon as the operation was completed, the deformed specimen was water quenched within 2-3 s in order to freeze the deformed microstructure.

Hydraulic press-forging tests were performed on a 250-ton triple-action hydraulic press. The operations were carried out in the temperature range 1223-1373 K in steps of 50 K and similar amount of strains were given at each temperature as mentioned in forge hammer operation. The calculated mean strain rate was equal to ≈ 0.22 s^{-1}.

The rolling operations were performed in a 2Hi/4Hi-instrumented laboratory rolling mill (Carl Wezel Model No. 420/350/275). The mill was fitted with a 2Hi hot-roller set, the roller being 420 mm in width and 350 mm in diameter. Tests were carried out in the temperature range 1173-1473 K (in steps of 100 K) at a roll speed of 16 rpm, and a true strain of 0.3 was achieved in a single step. The mean true strain rate during rolling was estimated using the following equation:

$$\dot{\varepsilon} = v\frac{\ln\left(\frac{h_0}{h}\right)}{\sqrt{R\Delta h}}, \qquad \text{(Eq 1)}$$

where ν is peripheral speed of the work roll = 16 rpm, R is the undeformed roll radius = 175 mm; h_0 is the thickness of the plate before rolling = 24 mm; h is the thickness of the plate after rolling = 18 mm; and $\Delta h = (h_0 - h)$. The calculated mean strain rate was found to be ≈ 2.6 s^{-1}.

2.3 Characterization

The hot worked samples were cut along the longitudinal direction and one half of the sample was taken to prepare metallographic specimens. The microstructures were examined optically in the maximum deformation zone of the samples and grain sizes were measured employing linear intercept method. Hardness measurements were carried out by Microhardness tester [HMV-2000 SHIMADZU] using 200-g load. The measurements were taken on the maximum deformation zone of the sample. Percentage recrystallization (%DRX) at different working conditions was calculated employing the following equation:

$$\%\mathrm{DRX} = \frac{H_{\mathrm{CW}(x)} - H_{\mathrm{HW}(x)}}{H_{\mathrm{CW}(x)} - H_{\mathrm{SA}}} \times 100, \qquad \text{(Eq 2)}$$

where $H_{\mathrm{CW}(x)}$ denotes the hardness of the cold worked specimen at a strain level of x percent, $H_{\mathrm{HW}(x)}$ is the hardness of the hot worked sample at same strain in a particular working temperature at which we want to find out the fraction of recrystallization, and H_{SA} denotes the hardness of solution annealed sample. To obtain $H_{\mathrm{CW}(x)}$, cold working operation of Alloy D9 at various strain levels were carried out by high strain rate compression testing machine at room temperature. Since Alloy D9 virtually does not soften by dynamic recovery (due to low to medium stacking fault energy), the above microhardness measurements method estimates the %DRX with sufficient accuracy and reliability. Similar approach, as depicted in Eq 2, have been adopted by Sakai et al. to evaluate the degree of softening in polycrystalline nickel after hot working employing flow stress value (Ref 7). Liu et al. have also employed similar hardness method to calculate the fraction of recrystallization in Al alloy (Ref 8).

3. Model Overview and Learning Algorithm

Artificial neural network is a highly simplified model of the structure of a biological network. The fundamental unit or building block of ANN is the processing element, also called an artificial neuron or simply a neuron. Some neurons interact with the real world to receive input, and some provide the real world with the output. Rest of the neurons remains hidden. Neurons are connected to each other by synapses; associated with each synapse is a weight factor. More details regarding ANN modeling can be found elsewhere (Ref 9).

In this study, a multilayer perceptron (MLP) based feed-forward ANN has been used since multilayer network has greater representational power for dealing with highly non-linear, strongly coupled, multivariable system (Ref 10). Although multilayer neural network does not ensure a global minimum solution for any given problem, it is a reasonable approximation that if the network is trained with a comprehensive database, the resulting model will approximate all of the laws of mechanics that the actual material or process obeys (Ref 11). A general scheme of the present ANN model is given in Fig. 1. The inputs of the model were strain (ε), strain rate ($\dot{\varepsilon}$) and temperature (T). The outputs of the model were microstructural features namely, %DRX and average grain size.[1] A total of 49 experimental dataset were used in the development

[1]There were two models, one for %DRX and another for average grain size. However, in the text sometimes the word "model" is used to refer to the two models collectively.

of the model. The metal-forming processes and corresponding data ranges are summarized in Table 2. All the data were normalized employing the relation given by,

$$x_N = \frac{x - x_{min}}{x_{max} - x_{min}} \quad \text{(Eq 3)}$$

where x_N is the normalized value of the parameter x; x_{max} and x_{min} are the maximum and minimum values of x, respectively; accordingly each parameter lies in the interval 0-1. The normalized dataset were then randomly divided into two groups. A total of 75% of the data were used for training and remaining for testing. A logistic sigmoid function expressed as Output $= (1 + e^{-\text{input}})^{-1}$ was employed as the activation function; the learning is based on gradient descent algorithm and hence requires the activation function to be differentiable. The convergence criterion for the network was determined by the average root-mean-square (RMS) error between the desired and predicted output values,

$$E_{RMS} = \frac{1}{N}\sum_{i=1}^{N}\sqrt{\frac{1}{p}\sum_{j=1}^{p}(d_{ji} - y_{ji})^2}, \quad \text{(Eq 4)}$$

where E_{RMS} is the average RMS, N is the number of training or testing data, p is the number of variables in the output, $d_j(n)$ and $y_j(n)$ are the target output and network output for neuron j, respectively. In all the calculations reported in this paper, a convergence criterion of 1% RMS error has been set. It was, however, found that the network invariably stabilizes before this criterion is met.

Instead of standard back propagation (BP algorithm), the network has been trained with some upgraded algorithms like Resilient propagation (Rprop) and Super self-adjusting back-propagation (superSAB). This is due to the fact that BP algorithm uses an instantaneous estimate for the gradient of error surface in weight space. The algorithm is therefore stochastic in nature, i.e., it has a tendency to zigzag its way about the true direction to a minimum on the error surface. Indeed, BP learning is an application of a statistical method known as stochastic approximation. Consequently, it tends to converge slowly and hence the back propagation networks with updated algorithms were used in the present study. A little description of the working of resilient propagation and superSAB algorithms is given below.

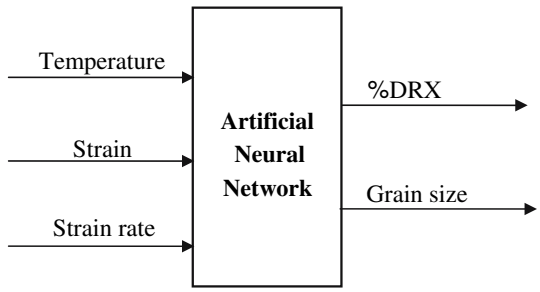

Fig. 1 Schematic of the ANN model for modeling microstructural evolution of Alloy D9

3.1 Resilient Propagation

Resilient propagation is an effective learning algorithm that is based on direct adaptation of the weight step based on local gradient information. It does not consider, different from standard back propagation, the harmful influence of the absolute value of the partial derivative for the calculation of weight changes, but only the sign of the derivative to indicate the direction of weight update. If the derivative is positive (increasing error), the weight is decreased by its update value. On the other hand, if the derivative is negative, the update value is added. The algorithm can be mathematically expressed as follow (Ref 12):

$$\Delta w_{ji}(n) = \begin{cases} -\Delta_{ji}(n), & \text{if } \frac{\partial E(n)}{\partial w_{ji}} > 0 \\ +\Delta_{ji}(n), & \text{if } \frac{\partial E(n)}{\partial w_{ji}} < 0 \\ 0, & \text{else} \end{cases} \quad \text{(Eq 5)}$$

$$w_{ji}(n+1) = w_{ji}(n) + \Delta w_{ji}(n)$$

$$\Delta_{ji}(n) = \begin{cases} \eta^+\Delta_{ji}(n-1), & \text{if } \frac{\partial E(n-1)}{\partial w_{ji}} * \frac{\partial E(n)}{\partial w_{ji}} > 0 \\ \eta^-\Delta_{ji}(n-1), & \text{if } \frac{\partial E(n-1)}{\partial w_{ji}} * \frac{\partial E(n)}{\partial w_{ji}} < 0 \\ \Delta_{ji}(n-1), & \text{else} \end{cases}, \quad \text{(Eq 6)}$$

where $0 < \eta^- < 1 < \eta^+$.

As can be seen from the Eq 5, the size of weight change is solely determined by the weight specific update value $\Delta_{ji}(n)$. Each time the partial derivative of the corresponding weight w_{ji} changes it sign, the $\Delta_{ji}(n)$ is decreased by a factor η^- (Eq 6), since it is indicated that the last update was too large and the algorithm jumped over a local minimum. On the other hand, if the derivative retains its sign, the update value is slightly increased by the factor η^+ in order to accelerate the convergence in shallow regions.

3.2 SuperSAB

The Super self-adjusting back-propagation (superSAB) algorithm is based on the idea of sign-dependant learning rate adaptation. The basic of the function is to change the learning rate exponentially instead of linearly. This is done in order to

Table 2 Ranges of the experimental data sets employed for ANN modeling in this study

Processes	Strain	Strain rate (s^{-1})	Temperature (K)
Forge hammer	0.1-0.5 (steps of 0.1)	100	1223-1423 (steps of 50 K)
Hydraulic press	0.1-0.5 (steps of 0.1)	0.22	1223-1373 (steps of 50 K)
Rolling	0.3	2.6	1173-1473 (steps of 100 K)

take the wide range of temporarily suited learning rates into account (Ref 13).

In case of a change in sign of two successive derivatives, the previous weight is reversed. SuperSAB algorithm is considered to be fast convergence algorithm. It has been shown that superSAB converges orders of magnitude faster than the original back propagation algorithm, and is only slightly instable (Ref 14).

4. Results and Discussion

4.1 Microstructural Evolution

The influence of strain on %DRX at various temperature levels during hammer forging and hydraulic press forging operation is shown in Fig. 2(a) and (b), respectively. It could be observed that, in general, %DRX increases with strain at a particular temperature level. One interesting behavior could be observed from Fig. 2(a) is that DRX was incomplete at 1423 K, though it has been found to be completed above 30% deformation level at 1373 K during forge hammer operation. In fact in this study, only these particular combinations of strain, strain rate, and temperature, DRX has been found to be completed. This behavior has been explained on the basis of a simple model of DRX in terms of rate of nucleation vs. rate of grain boundary migration (Ref 3). Alloy D9 is a low to medium staking fault energy (SFE) material. Therefore, rate

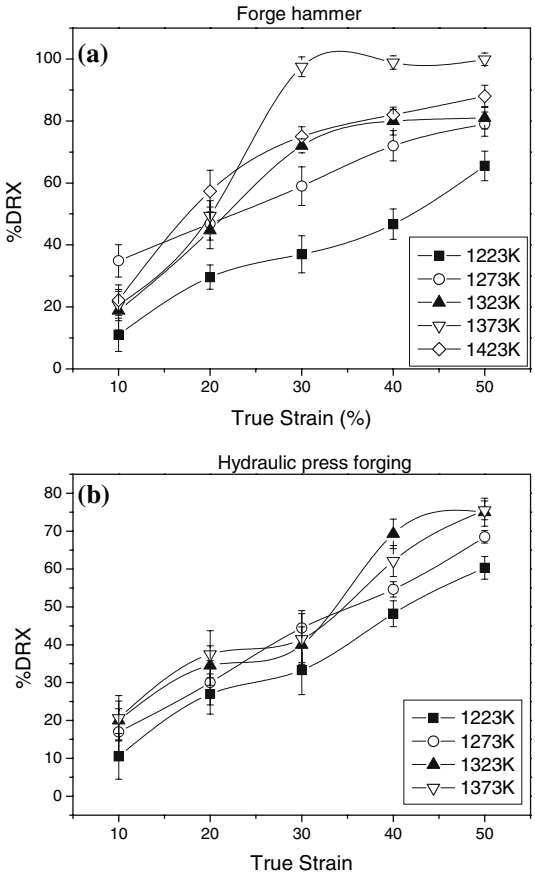

Fig. 2 Influence of strain on %DRX during (a) forge hammer, (b) hydraulic press forging operation

of nucleation would dominate over grain boundary migration (Ref 15). The rate of nucleation could be expressed as,

$$\dot{N} = (\beta\dot{\varepsilon}/bl)\exp[-Q/RT], \quad \text{(Eq 7)}$$

where β = constant, $\dot{\varepsilon}$ = strain rate, b = Burgers vector, l = dislocation segment length, Q = activation energy for diffusion, R = gas constant, and T = temperature. Since Alloy D9 is basically a Ti modified stainless steel, TiC precipitates were likely to take place in the matrix during straining. These precipitates would pin the dislocations and thereby reduced the link length 'l' (Eq 7) which eventually favored DRX. TiC precipitates, in fact, were found to facilitate DRX in Alloy D9 with Ti/C ratio of 8 where the extent of DRX was found much higher as compared to Alloy D9 with zero Ti at identical processing conditions (Ref 16). However, if the processing temperature becomes too high, dissolution of these precipitates would happen; thereby the favorable conditions of DRX offered by precipitates would be substantially lost. In yet another study by the authors on the effect of annealing temperatures in the range 1323-1573 K on engineering properties for Alloy D9, it was found that the amount of precipitates decreased with increasing annealing temperature (Ref 17). From the present study, it seems 1373 K was the optimum processing temperature for Alloy D9 where the complicated interactions between precipitates and processing parameters (i.e., strain, strain rate, and temperature) were just sufficient to complete the DRX process. On the other hand, 1423 K was a higher range of temperature where dissolution of the TiC precipitates might take place; thereby the rate of nucleation would be lowered despite the fact that available thermal activation energy was more as compared to 1373 K.

The microstructural evolution during forge hammer operation is shown in Fig. 3. At low temperature and low strain (Fig. 3(a)), the microstructure consisted of big parent grains and lamella like straight annealing twins. The dynamically recrystallized grains were hardly found in the matrix. The bulging of parent grain boundary and subsequent evolution of 'necklace' structure (shown by arrow) could be observed in Fig. 3b. Bulging of grain boundaries was frequently observed as a prelude to DRX. The evolution of necklace type microstructure during initial stage of DRX has been reported by several researchers in a variety of low to medium stacking fault energy materials including austenitic stainless steels (Ref 18, 19). At higher temperature and strain level, the deformed grain structures have almost been disappeared and microstructure consisted of small equiaxed recrystallized grains (Fig. 3(c)).

As could be seen from the micrographs, grain size evolution during DRX is complex in nature. When the extent of DRX was negligible (Fig. 3(a)), micrograph shows a single peak distribution of parent grains. However, at a higher extent of DRX, a clear bimodal distribution of grains could be observed (Fig. 3(b)). Some of these grains are equiaxed in nature while the others are elongated parent grains. Finally, again single peak distributions of new equiaxed dynamically recrystallized grains were observed when the DRX process was almost completed (Fig. 3(c)). It is, therefore, clear that grain size distributions and aspect ratios are required in order to truly represent the DRX grains. However, this necessitates to include more input neurons in the neural network, which would result in increased number of connection weights in the model. This would require more experimental data than that was considered

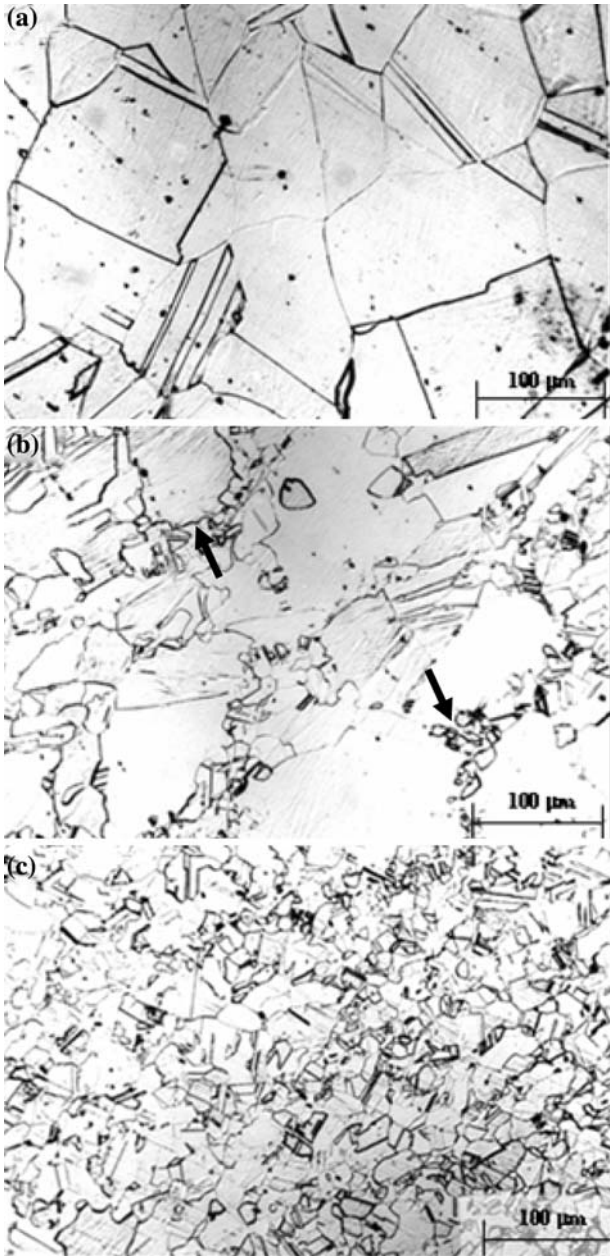

Fig. 3 Optical micrograph of alloy D9 during forge hammer operation (a) $T = 1223$ K, $\varepsilon = 0.07$, (b) $T = 1273$ K, $\varepsilon = 0.28$, (c) $T = 1423$ K, $\varepsilon = 0.46$

in the present study. Therefore, we have considered the average grain size (along with the fraction of DRX) for the model with out losing relevant information about the developed microstructure.

4.2 Neural Network Results

One hidden layer was found to be adequate for the present problem. This observation reaffirms the universal approximation theorem that a single-layer of non-linear hidden units is sufficient to approximate any continuous function. Hornik et al. (Ref 20) have also shown that a three-layer ANN with sigmoid transfer function can map any function of practical interest. Neurons in the hidden layer were varied from 1 to 15. Neurons more than 15 were not tried in order to avoid over fitting. The

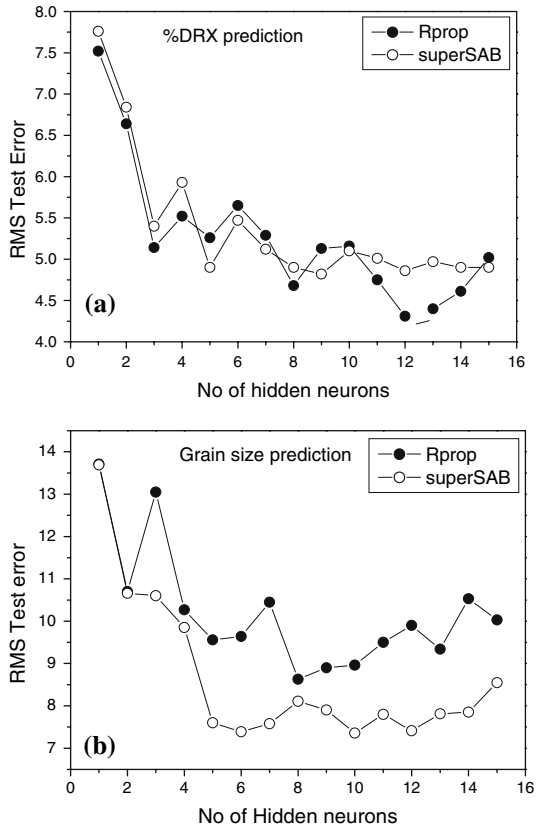

Fig. 4 Performances of the ANN model at various hidden neurons level for (a) %DRX, (b) grain size prediction

performance of the model for %DRX and grain size prediction at different hidden neuron level is shown in Fig. 4(a) and (b), respectively. It could be observed from Fig. 4(a) that an ANN model with 12 hidden neurons and Rprop algorithm produced best performance for %DRX prediction. On the other hand, an ANN model with 10 hidden neurons and superSAB algorithm yielded best performances for grain size prediction (Fig. 4(b)).

A wide variety of standard statistical performance evaluation measures have been employed to quantify the model performance. Along with the RMS error, the predictability of the network was quantified in terms of correlation coefficient (R) and scatter index (SI). These are defined below.

$$R = \frac{\sum_{i=1}^{N}(E_i - \bar{E})(P_i - \bar{P})}{\sqrt{\sum_{i=1}^{N}(E_i - \bar{E})^2 \sum_{i=1}^{N}(P_i - \bar{P})^2}} \quad \text{(Eq 8)}$$

$$\text{SI} = \frac{E_{\text{RMS}}}{\bar{E}} \quad \text{(Eq 9)}$$

where E is the experimental finding and P is the predicted value obtained from the neural network model. $\bar{E}$ and $\bar{P}$ are the mean values of E and P, respectively. N is the total number of data employed in the investigation. E_{RMS} is the average RMS error given by Eq 4. The salient features and the performances of the models are depicted in Table 3. It could be suggested that both resilient propagation and superSAB algorithm can efficiently predict the microstructural features with reasonable accuracy

Table 3 The salient features and performances of the model for %DRX and grain size prediction in alloy D9

Output variable	Learning algorithm	Hidden neurons	RMS test error (%)	*R*	SI	Iterations
%DRX	Rprop	12	4.31	0.984	0.079	400
	superSAB	9	4.82	0.975	0.088	2400
Grain size	Rprop	8	7.83	0.945	0.093	500
	superSAB	10	7.36	0.952	0.081	2700

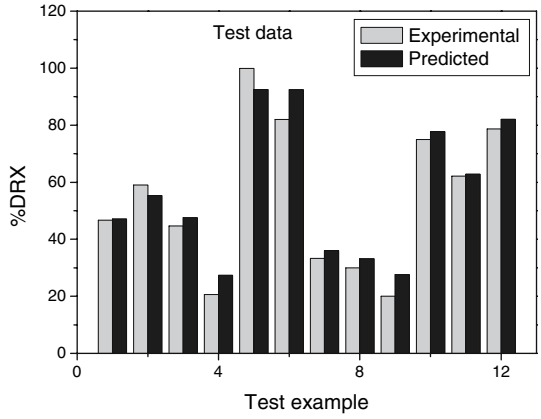

Fig. 5 Accuracy of the ANN model prediction of %DRX, when compared with experimental data

and reliability. However, most striking outcome of this analysis was that the resilient propagation required less number of iterations and therefore it showed a faster convergence (~6 times faster) as compared to superSAB.

4.2.1 %DRX Prediction. The comparison between experimental and predicted test data for %DRX is shown in Fig. 5. Since test data were not used for training, it essentially verified the ability of any ANN model to associate and generalize a true physical response, which is unknown to the network. As can be seen, experimental findings are close to the predicted ones. The magnitude of the error in prediction is less than the errors that normally arises in %DRX measurements as shown by error bar in Fig. 2. Therefore, it could be efficiently applied for further simulation and application. It should be reiterated here that the designed models are 'statistical' models, i.e., they are not based on any physical theories. Thereby simulated results from the models have been explained by relevant fundamental metallurgical phenomena.

The combined influence of strain and temperature on %DRX is shown in Fig. 6. It could be noticed that DRX was essentially strain dominated especially at the lower strain rate, i.e., in hydraulic press forging operation (Fig. 6(b)). With increased of both the strain and temperature, %DRX increased. This behavior could be well explained from the theory of recrystallization. It is well known fact that defects are the nucleating sites for formation of new strain free grains during recrystallization. With increase in strain, the amount of stored energy and the number of defects with in the crystal lattice increase. So the defect density with in the crystal increases that ultimately leads to more amount of DRX. On the other hand, the microscopic mechanisms controlling recrystallization are thermally activated. With increase in temperature, the available thermal activation energy for high angle grain boundary migration increases. This eventually favors nucleation and subsequent expansion of DRX.

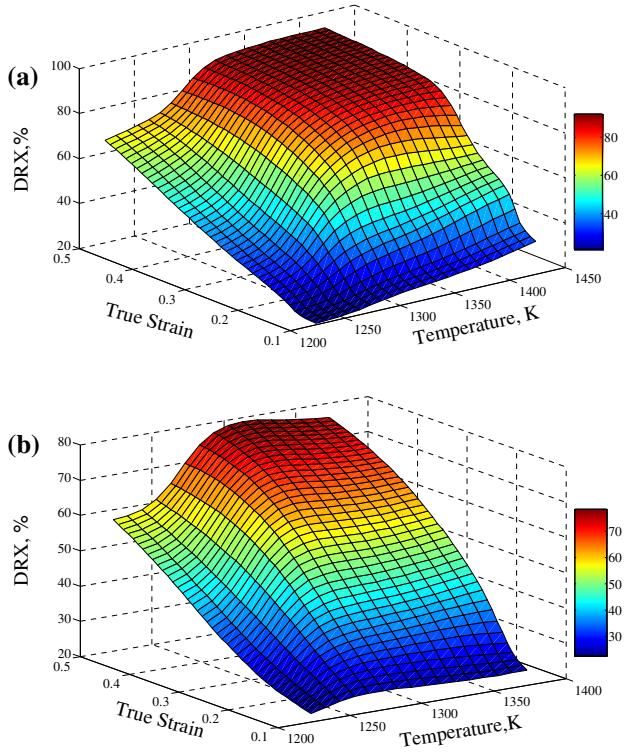

Fig. 6 Combined influence of temperature and strain on %DRX during (a) forge hammer, (b) hydraulic press forging operation

A close look in Fig. 6 revealed that our ANN model never predicted 100% DRX. However, it has been already discussed (Section 4.1) that DRX has been completed above 30% deformation level at 1373 K during forge hammer operation due to complicated interactions between precipitates and processing parameters. Therefore, it is clear that our model could not able to track the effect of precipitates on DRX. This could be attributed to the lack of input information or insufficient amount of data to the network regarding the effect of precipitation on DRX. Another important observation is made from Fig. 6(b) is that ~80% DRX is obtained during hydraulic press forging at the maximum temperature and strain which is essentially much lower than that achieved during forge hammer operation. The results have been found to be consistent with the experiments (Fig. 2(b)). The reason could be attributed to the lower strain rate of hydraulic press. As the strain rate for hydraulic press is low, the time taken to complete the specified deformation was relatively high. This would result in a temperature drop that reduced the thermal activation energy for nucleation and subsequent expansion of DRX. Thereby, DRX process could not be completed even at maximum temperatures and strains during hydraulic press forging.

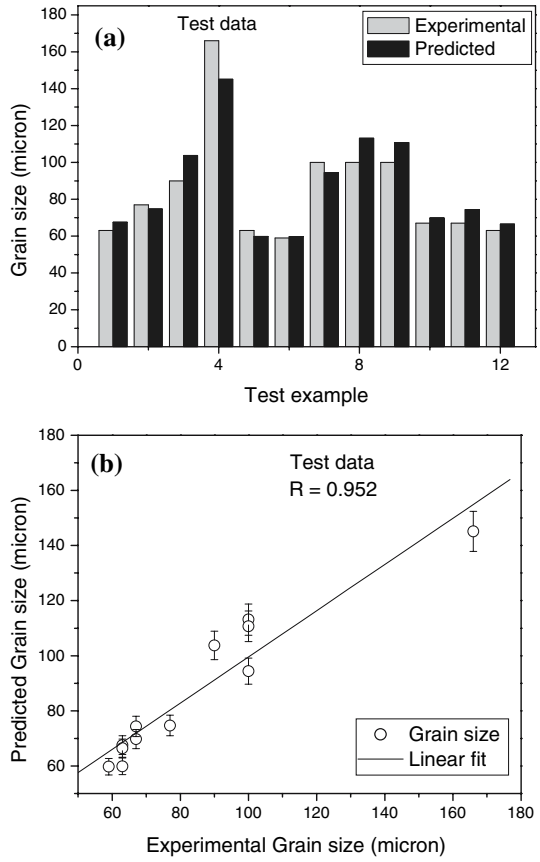

Fig. 7 Accuracy of the ANN model for grain size prediction (a) direct comparison, (b) regression analysis

4.2.2 Grain Size Prediction. The performance of the model for grain size prediction is shown in Fig. 7. It could be observed from Fig. 7(a) that the experimental data are much closer to the predicted data. The correlation between experiments and predicted results for same database has been shown by regression analysis in Fig. 7(b). It could be observed that correlation is fairly good. The deviation in correlation is about 5% and is shown by error bar. Figure 7(b) revealed that the prediction is quite accurate for the lower grain size range, which corresponds to complete recrystallization (single peak distribution). A slight underestimation could be observed for the higher grain size, which also corresponds to single peak distribution of parent grains. However, for the grain sizes in the range 80-100 μm, the deviation in prediction is significant. This may be due to the bimodal distribution of grains in this range as discussed earlier. However, this magnitude of the error in prediction, in fact, is less than the error that normally arises during grain size measurement. So the developed model could be applied for grain size prediction with reasonable accuracy.

The combined influence of strain and temperature on average grain size evolution is shown in Fig. 8. Almost similar trend has been observed for hydraulic press forging and rolling operation and thereby not reiterated here. It could be observed that with increase of both the temperature and strain, grain size decreases. This happened due to concomitant grain refinement during DRX. It has already mentioned the DRX accelerated at high temperature and strain. This eventually leads to lower grain size in the product microstructure.

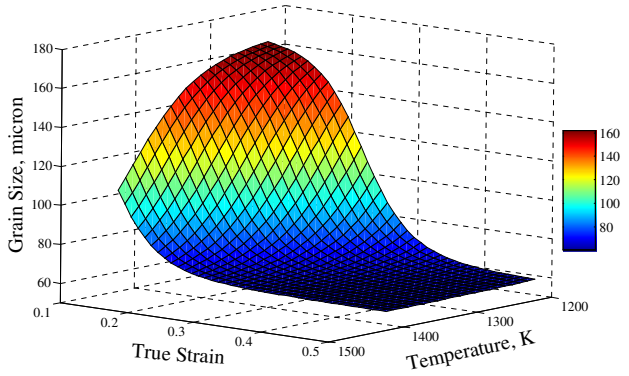

Fig. 8 Combined influence of temperature and strain on grain size during Forge hammer operation

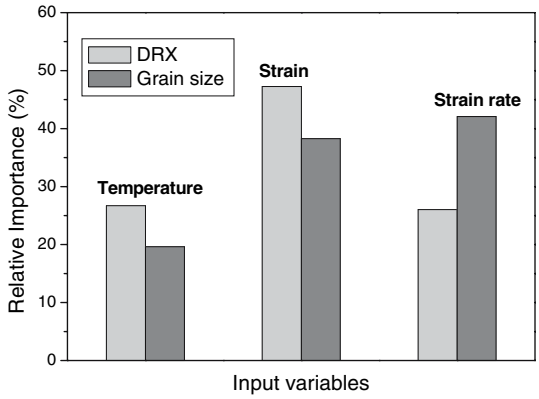

Fig. 9 Relative importance of the input parameters on microstructural evolution of alloy D9 during DRX

4.2.3 Sensitivity Analysis. Sensitivity analysis was carried out to determine the relative importance of the individual input parameter on microstructural evolution during DRX of Alloy D9. Though various approaches have been proposed and adopted to quantify the relative importance of input variables (Ref 21-23), the algorithm proposed by Garson (Ref 24) and repeated by Goh (Ref 25) is found to be the most robust in this respect. In this present study, relative importance of the input variables was determined employing this algorithm. The method essentially involves partitioning the hidden-output connection weights into components associated with each input neuron using absolute values of connection weights. The algorithm works based on the following principles:

(i) The absolute value of each hidden-output connections weights w_k, $k = 1, 2, \ldots\ldots, h$ incorporated into the input-hidden connection weights w_{ij} to yield partitions w_{ij}^* using the following expression:

$$w_{ij}^* = \frac{|w_{ij}|}{S_j} \times |w_k| \quad \text{(Eq 10)}$$

$$S_j = \sum_{i=1}^{p} |w_{ij}| \quad \text{(Eq 11)}$$

where $i = 1, 2, \ldots, p$ and $j = 1, 2, \ldots, h$.

(ii) For each input neuron, the adjusted weight w_{ij}^{*} are summed over all the hidden neurons and converted into percentage of the total for all input neurons. This percentage value serves as the relative importance of each input variable.

The relative importance of individual input parameters on microstructural evolution of Alloy D9 is shown in Fig. 9. It could be observed that strain is the most sensitive parameter for DRX while both strain and strain rate contribute substantially for grain size. It has already been demonstrated that DRX of Alloy D9 is essentially a strain-dominated process especially at the lower strain rate, i.e., in hydraulic press forging operation. The higher influence of strain rate on grain size arised due to the temperature loss during lower strain rate, i.e., in hydraulic press forging operation.

5. Conclusions

Artificial neural network model has been developed to predict the microstructural evolution of Alloy D9 during DRX. The input parameters were strain, strain rate, and temperature whereas microstructural features namely, %DRX and average grain size were the output parameters. Instead of standard BP algorithm, the network has been trained with two upgraded algorithms namely, Rprop and superSAB. Both the algorithms predicted the microstructural features with reasonable accuracy and reliability. However, Rprop was found to have a faster convergence compared to superSAB in the present investigation. The performance of the model was evaluated using a wide variety of statistical indices. A good agreement between experimental and predicted data was obtained. The influence of temperature and strain on microstructural features have been simulated by employing the developed model. The results were found to be consistent with the metallurgical trends. An instantaneous microstructure, therefore, can be predicted from the developed ANN model as a function of process parameters during DRX of alloy D9.

Acknowledgments

The authors would like to express their sincere thanks to Dr. S. Venugopal, Head, Metal Forming & Tribology Section and Dr. S.K. Ray, Head, Materials Technology Division for useful discussions. The authors also gratefully acknowledge Dr. Baldev Raj, Director, Indira Gandhi Centre for Atomic Research (IGCAR) for his constant encouragement throughout the course of this work.

References

1. R.W. Cahn and P. Haasen, *Physical Metallurgy*, Vol. III, 4th ed., North Holland, 1996
2. T. Sakai and J.J. Jonas, Dynamic Recrystallization: Mechanical and Microstructural Considerations, *Acta Metal.*, 1984, **32**(2), p 89–209
3. S. Mandal, P.V. Sivaprasad, and R.K. Dube, Kinetics, Mechanism and Modelling of Microstructural Evolution During Thermomechanical Processing of a 15Cr-15Ni-2.2Mo-Ti Modified Austenitic Stainless Steel, *J. Mater. Sci.*, 2006, **42**, p 2724–2734
4. C.M. Sellars, Modeling Microstructural Development During Hot Rolling, *Mater. Sci. Technol.*, 1990, **15**, p 1072
5. M.F. Ashby, Physical Modeling of Materials Problem, *Mater. Sci. Technol.*, 1992, **8**, p 102
6. T.W. Kim and F.P.E. Dunne, Modeling Heterogeneous Microstructure in Superplasticity, *Proc. R. Soc. Lond. A Math. Phys. Sci.*, 1999, **455**, p 719
7. T. Sakai, M. Ohashi, K. Chiba, and J.J. Jonas, Recovery and Recrystallization of Polycrystalline Nickel After Hot Working, *Acta Metal.*, 1988, **36**(7), p 1781–1790
8. W.C. Liu and J.G. Morris, Effect of Initial Texture on the Recrystallization Texture of Cold Rolled AA 5182 Aluminum Alloy, *Mater. Sci. Eng. A*, 2005, **402**(1–2), p 215–227
9. S. Haykin, *Neural Networks: A Comprehensive Foundation*. Prentice Hall, Upper Saddle River, New Jersey, 1999
10. S.C. Juang, Y.S. Tarang, and H.R. Lii, A Comparison Between the Back-Propagation and Counter-Propagation Networks in the Modeling of the TIG Welding Process, *J. Mater. Process. Technol.*, 1998, **75**(1–3), p 54–62
11. M.S. Chun, J. Biglou, J.G. Lenard, and J.G. Kim, Using Neural Networks to Predict Parameters in the Hot Working of Aluminum Alloys, *J. Mater. Process. Technol.*, 1999, **86**(1–3), p 245–251
12. M. Riedmiller and H. Braun, *A Direct Adaptive Method for Faster Back Propagation Learning: The RPROP Algorithm*. Proceedings of International Conference in Neural Networks, San Francisco, CA, 1993
13. M. Riedmiller, Advanced Supervised Learning in Multi-layer Perceptrons - From Backpropagation to Adaptive Learning Algorithms, Special Issue on Neural Networks, *Int. J. of Comp. Stand. Inter.,* 1994, **16**, p 265–278
14. T. Tollenaere, SuperSAB: Fast Adaptive Back Propagation with Good Scaling Properties, *Neural Network*, 1990, **3**(5), p 561–573
15. Y.V.R.K. Prasad and N. Ravichandran, Effect of Stacking Fault Energy on the Dynamic Recrystallization During Hot Working of FCC Metals: A Study Using Processing Maps, *Bull. Mater. Sci.*, 1991, **14**, p 1241–1248
16. S. Mandal, P.V. Sivaprasad, S. Venugopal, and K.P.N. Murthy, Constitutive Flow Behaviour of Austenitic Stainless Steels Under Hot Deformation: Artificial Neural Network Modeling to Understand, Evaluate and Predict. *Model. Simul. Mater. Sci. Eng.*, 2006, **14**, p 1053
17. S. Venugopal, P.V. Sivaprasad, and S. Venkadesan, Effect of Annealing Temperature on Engineering Properties of Alloy D9, Unpublished Work
18. D. Ponge and G. Gottstein, Necklace Formation During Dynamic Recrystallization: Mechanisms and Impact on Flow Behavior, *Acta Mater.*, 1998, **46**(1), p 69–80
19. E. Brunger, X. Wang, and G. Gottstein, Nucleation Mechanisms of Dynamic Recrystallization in Austenitic Steel Alloy 800H, *Scripta Mater.*, 1998, **38**(12), p 1843–1849
20. K. Hornik, M. Stinchcombe, and H. White, Multilayer Feed Forward Networks are Universal Approximations, *Neural Network*, 1989, **2**(5), p 359–366
21. J.D. Olden and D.A. Jackson, Illuminating the "Black Box": A Randomization Approach for Understanding Variable Contributions in Artificial Neural Networks, *Ecol. Model.*, 2002, **154**(1–2), p 135–150
22. M. Gevrey, I. Dimopoulos, and S. Lek, Review and Comparison of Methods to Study the Contribution of Variables in Artificial Neural Network Models, *Ecol. Model.*, 2003, **160**(3), p 249–264
23. J.D. Olden, M.K. Joy, and R.G. Death, An Accurate Comparison of Methods for Quantifying Variable Importance In Artificial Neural Networks Using Simulated Data, *Ecol. Model.*, 2004, **178**(3–4), p 389–397
24. G.D. Garson, Interpreting Neural Network Connection Weights, *Artif. Intell. Expert*, 1991, **6**(7), p 47–51
25. A.T.C. Goh, Back-Propagation Neural Networks for Modelling Complex Systems, *Artif. Intell. Eng.*, 1995, **9**, p 143–151